Graphical Abstract

https://doi.org/10.1016/j.cej.2021.129618

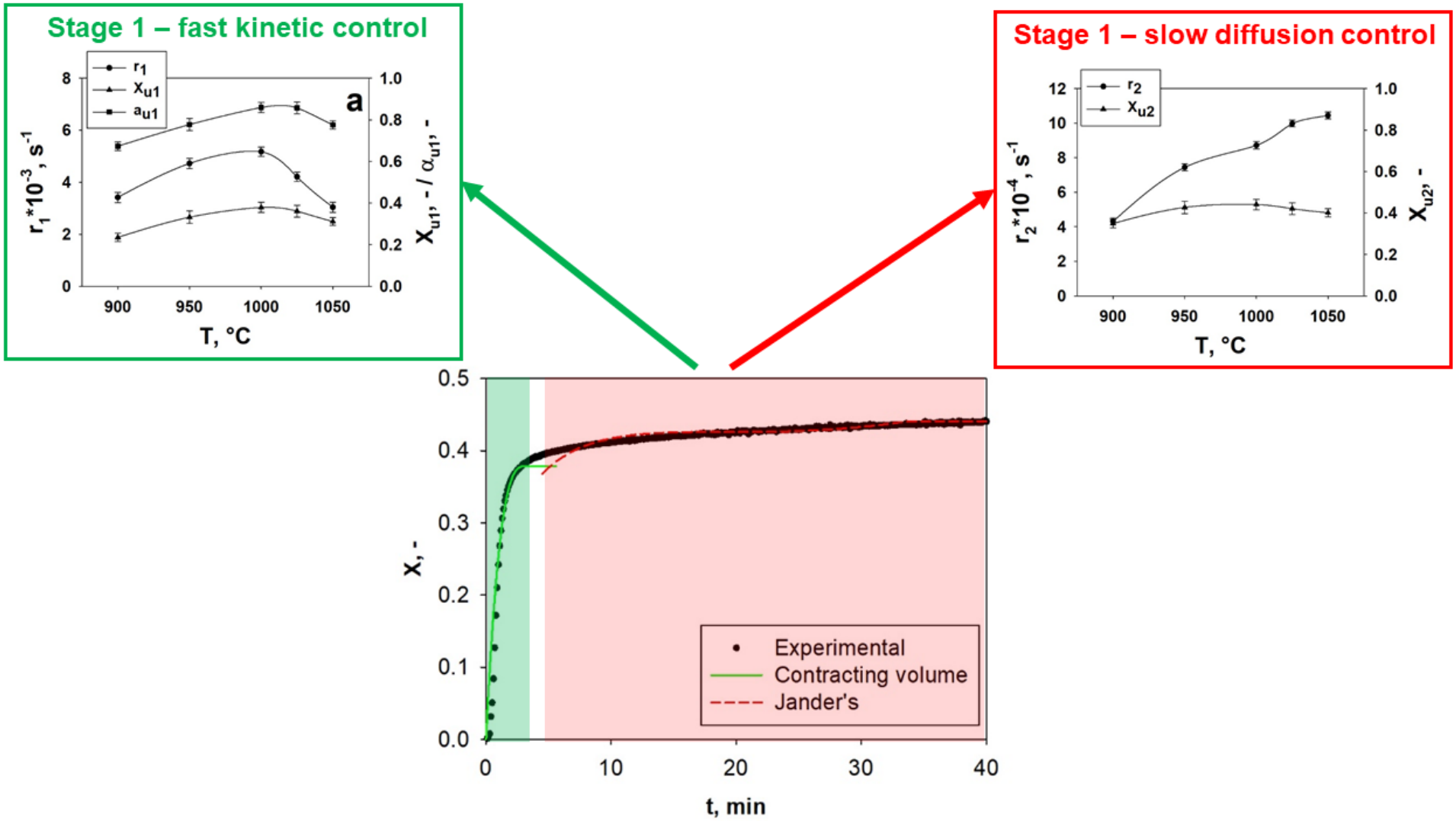

https://doi.org/10.1016/j.cej.2021.129618

Highlights

1. The carbonation kinetics of a SrO-Al_2O_3 composite has been investigated for TCES-CSP
2. SrO has been stabilized using Al_2O_3 as a sintering/agglomeration inhibitor
3. The fast carbonation stage is well described by the contracting volume model
4. The slow carbonation stage is well described by the Jander's model
5. Activation energy of the SrO-Al_2O_3 carbonation reaction at the 900-1000°C was estimated as 52 kJ/mol.

https://doi.org/10.1016/j.cej.2021.129618

Kinetics of the Carbonation Reaction of an $SrO-Al_2O_3$ Composite for Thermochemical Energy Storage

Paola Ammendola[a], Federica Raganati[a,*], Elena Landi[b], Annalisa Natali Murri[b], Francesco Miccio[b]

[a]Istituto di Scienze e Tecnologie per l'Energia e la Mobilità Sostenibili (STEMS) - CNR, Piazzale Tecchio 80, 80125 Naples, Italy

[b]Istituto di Scienza e Tecnologia dei Materiali Ceramici (ISTEC) - CNR, via Granarolo, 64, 48018 Faenza, Italy

*Corresponding author

Tel.:+39 0817682237; fax:+39 0815936936.

E-mail address: federica.raganati@stems.cnr.it

ABSTRACT

In framework of the thermochemical energy storage (TCES) in concentrating solar power (CSP) applications, great attention is focused on the $SrCO_3$/SrO system, which is characterized by remarkably high theoretical volumetric energy density (4 GJ $m_{SrCO_3}^{-3}$) and working temperatures (1200 °C). It has been shown that the incorporation of Al_2O_3 in the SrO/$SrCO_3$ system can successfully hinder the sintering and agglomeration phenomena, thus improving the performances of the system. Aiming at providing useful information for the design, simulation and scale up of a reactor for the energy storage, besides the multicycle carbonation conversion, the evaluation of the reaction kinetics is crucial.

Thus, in this work, the kinetics of the carbonation of a SrO-Al_2O_3 composite (34%wt of Al_2O_3) for TCES-CSP has been investigated, for the first time using a two-stage kinetic model. In particular, tests have been performed in a thermogravimetric analyzer at operating conditions relevant for TCES, namely at 1 atm of CO_2 partial pressure within the temperature range of 900 °C – 1050 °C. The reaction rate, the intrinsic carbonation kinetic constant, the characteristic product layer thickness and their dependence on the temperature has been evaluated in the temperature range 900 – 1000 °C; the activation energy has been found to be 52 kJ mol-1. Finally, comparison of the calculated conversion-time profiles, obtained from the applied kinetic models, with experimental data revealed a good agreement.

Keywords: Thermochemical Energy Storage (TCES); Concentrating Solar Power (CSP); Carbonation kinetics; Strontium oxide.

1. Introduction

One of the main advantages of concentrated solar power (CSP) generation combined with thermal energy storage (TES) is the dispatchability, i.e. the capacity to provide energy upon demand (peak), or alternatively, to store energy in weak periods [1]. Nonetheless, much research effort is still needed in the field of energy storage for CSP to become competitive with photovoltaics and other renewable power sources [2,3]. In this framework, TES systems can be improved, in terms of both the efficiency and economic competitiveness, if the plant is operated at temperatures higher than 600 °C, with practical advantages by virtue of the second law of thermodynamics and Carnot efficiency [4].

Several technological approaches may be used to perform TES, depending on the way the heat storage is accomplished: sensible thermal energy storage (STES), latent thermal energy storage (LTES) and thermochemical energy storage (TCES) [5–7]. In this context, TCES, consisting in storing energy in the form of enthalpy of reversible reactions, is one of the most promising alternatives since it can provide several benefits with respect to the other alternatives: high volumetric energy density (1 GJ m^{-3}), high working temperatures (> 600 °C), non-toxic reactants [8,9]. So far, several reactive systems have been proposed for TCES applications, such as metallic hydrides, carbonates, hydroxides and reducible oxide system [8,9]. Among these, alkaline-earth metal oxides/carbonates can provide the highest theoretical volumetric energy density (up to 4 GJ $m^{-3}_{carbonate}$) and storage temperature (typically > 800°C) [9,10]. Therefore, a TCES system based on the carbonation/calcination looping can be carried out so that: the endothermic calcination reaction is the solar-driven step in which the metal oxide is produced; this metal oxide is, then, carbonated in the exothermic step from which thermal energy is released and used to drive a thermodynamic cycle for power generation [4].

Among all the possible alkaline metal oxides/carbonates couples, the $CaO/CaCO_3$ one, characterized by an energy density of 3.26 GJ $m^{-3}_{CaCO_3}$ and a dissociation temperature at atmospheric conditions of 895 °C, has been deeply studied for the calcium looping process to be applied in the framework of both CO_2 capture and storage (CCS) [11,12] and TCES applications [13,14]. Regardless of the

specific applications (either CCS or TCES), carbonate looping cycles are typically carried out in fluidized bed reactors [11,13,14], due to the high heat/mass transfer coefficients and uniformity of temperature they can typically provide [3,15–18]. It is important to underline that the optimum conditions to carry out the calcium looping process strongly depend on the particular application [19]. In fact, in the case of CCS applications: the calcination, whose conditions are dictated by the need of extracting from the calciner high-concentration CO_2 stream to be compressed and sequestered, is performed at high temperature (~950 °C) under high CO_2 partial pressure [19,20]. The carbonation, whose conditions are dictated by the fixed concentration of the combustion flue gases, is performed under low CO_2 partial pressure (~0.15 bar) at the lowest possible temperature (~650 °C) able to favor the reaction thermodynamically [19,20]. In the case of TCES applications: since there is no more CO_2 capture/storage issue, relatively low temperatures (~750 °C) and CO_2 partial pressures (P_{CO_2} = 0 bar, i.e., by using a gas easily separable from CO_2, such as superheated steam or helium) may be employed to perform the calcination. On the contrary, aiming at achieving high global efficiency for energy storage and electricity generation, high CO_2 partial pressures and temperatures (around or above 800 °C) [19,20]. Of course, using He for calcination would require the separation of the He/CO_2 gas mixture exiting from the calciner, that could be carried out relatively easily by means of selective membranes due to the differences in molecular size of helium (similar to H_2) and CO_2 [21]. It should be taken into account that the need also exists to realize a process characterized by free CO_2 emissions. To this aim, the CaL-CSP will be performed according to a closed cycle scheme, as thoroughly discussed by Chacartegui et al. [21]. In this configuration a pure CO_2 stream is fed to the carbonator with a molar rate well above the stoichiometric needs for carbonation. The excess CO_2 leaving the carbonator is used as heat carrier fluid to remove the heat released during carbonation and sent to a gas turbine for power production by means of a CO_2 closed Brayton cycle. Then it is compressed and stored for the successive cycles. Of course, the fact that this scheme is a closed cycle implies that it does not require the plant to be continuously fed by any gas stream, which applies also and especially in the case of helium, which is a very expensive gas [21].

Similarly to the well-known $CaO/CaCO_3$ system, also the $SrO/SrCO_3$ couple has been attracting growing attention due its advantageous characteristics [4,22–25]. In this case, the reaction scheme is:

$$SrCO_3 \rightleftharpoons SrO + CO_2 \qquad \Delta H^0_{rxn} = 234\ KJmol^{-1} \qquad (1)$$

The thermodynamics of the system is strongly dependent on the CO_2 partial pressure P_{CO_2} [23]. Fig. 1 reports the equilibrium P_{CO_2} ($P^{eq}_{CO_2}$), during the carbonation-calcination reaction shown in Eq. (1) at temperature between 900 °C and 1200 °C.

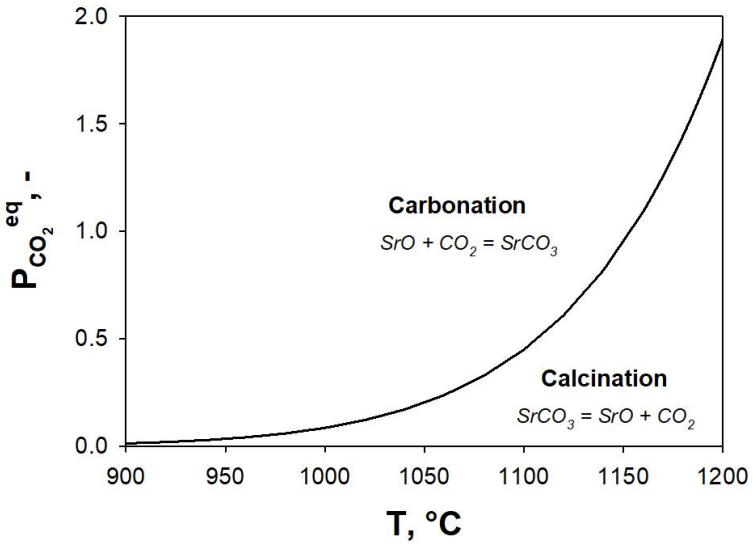

Fig. 1. CO_2 pressure as function of the temperature for the SrO-$SrCO_3$ system at thermodynamic equilibrium.

In particular, $P^{eq}_{CO_2}$ is equivalent to equilibrium constant and, therefore, it can be calculated as:

$$P^{eq}_{CO_2} = exp\left(-\frac{\Delta G^0_{rxn}(T)}{RT}\right) \qquad (2)$$

where R is the universal gas constant, T is the temperature and $\Delta G^0_{rxn}(T)$ is the standard state Gibbs free energy change for the reaction at temperature T, evaluated from tabulated thermochemical data [26]. Clearly, Fig. 1 suggests that increasing values of $P^{eq}_{CO_2}$ at a constant temperature or decreasing the temperature at a constant $P^{eq}_{CO_2}$ favors the carbonation reaction thermodynamically, i.e. thus resulting in a greater SrO carbonation conversion.

Being Sr the 15th most abundant element of earth, $SrCO_3$ is readily available and rather inexpensive [22]. Besides that, $SrCO_3$ is characterized by higher energy density (4 GJ $m_{SrCO_3}^{-3}$) and dissociation temperature (which occurs at temperature higher than the equilibrium temperature, 1175 °C at P_{CO_2} = 1atm [23]), thus being able to provide a higher quality of heat release in a still technologically feasible temperature range [22]. In spite of these favorable features, this system suffers from the same critical weakness affecting $CaO/CaCO_3$, namely the dramatic loss of SrO reactivity after multiple carbonation/calcination cycles, which is caused by sintering phenomena [4,23,24]. In this framework, different methods have been proposed to mitigate the sintering deactivation of the sorbents for looping applications, such as improved synthesis methods, supplementary treatments of the sintered sorbents (such as hydration treatment, thermal pretreatment and chemical pretreatment) and incorporation of refractory inert particles (e.g. Al_2O_3, SiO_2, TiO_2, ZrO_2, Y_2O_3 and MgO) [27,28]. For example Gigantino et al. [28] investigated the cycling stability of MgO-stabilized SrO samples produced with different precursors, support contents and production methods and found that the best performance was obtained by using the wet-mixing method with strontium acetate hemihydrate and porous magnesium oxide as precursors. Likewise, as a possible solution to the sintering deactivation of SrO, different Authors also assessed the use of additives with great thermal stability to inhibit the sintering stress by acting as "spacers", i.e. by physically separating the sorbent particles [23,24]. So far, Rhodes et al. [24] tested the $SrO/SrCO_3$ system supported by zirconia-based sintering inhibitors by thermo-gravimetric analysis, showing that it can provide a good repeatability of the weight loss over dozens of cycles. Likewise, Bagherisereshki et al. [23] successfully proposed the addition of $CaSO_4$ and $Sr_3(PO_4)_2$ to the $SrO/SrCO_3$ system to limit the sintering phenomena. Miccio et al. [25,29], under fixed bed conditions for CCS application, and more recently Ammendola et al. [30], under fluidized bed conditions for TCES applications, verified that of Al_2O_3 can be effectively used as sintering/agglomeration inhibitor.

Even though much research activity [4,23,24] has been devoted to the analysis and contrast of the decrease of the SrO carbonation conversion over repeated carbonation/calcination cycles, no studies

are available on the kinetic modelling of the SrO carbonation reaction under operating conditions typical of TCES-CSP applications. However, it is a matter of fact that reaction kinetics is a key point when reactors for thermal processes must be designed and scaled-up from laboratory to real scale [31]. Indeed, regardless of the specific configuration (packed, moving, fluidized bed, etc.), the design and scale-up of the reactor is based on calculation of required residence times which are strictly dependent on inherent kinetic parameters of the carbonation reaction.

In this framework, it should be remarked that peculiar reaction conditions, which directly affect the sorbent performance (in terms of both multicycle conversion and kinetics), are needed for the carbonation/calcination looping [32]. In this regard, a huge number of studies are focused on the carbonation kinetics of CaO at operating conditions functional to CCS applications [33–39], only few deal with the CaO [32,40] and SrO [20] carbonation kinetics at TCES-CSP operating conditions.

It is well-known that carbonation, as a typical gas–solid reaction producing a solid product, occurs in two phases characterized by two different kinetic regimes [14]. In the first stage (stage 1) the carbonation occurs through a fast chemical reaction of the CO_2 molecules with the fresh oxide surface [14]. Then, a thin layer of carbonate covers the free surface of the sorbent particles, after the fast kinetically-controlled stage, and the reaction rate shifts to be controlled the diffusion of CO_2 molecules through this solid layer (stage 2) [14]. In this framework, the thickness of the product layer is a critical parameter for understanding the carbonation reaction during the fast and slow reaction periods and the transition between these two kinetic stages of the reaction [41].

In this work, the carbonation kinetics of an SrO-Al_2O_3 composite (34%wt of Al_2O_3) has been studied for TCES-CSP in a thermogravimetric analyzer for the first time. In particular, since the carbonation behavior, in terms of both mutlicyclic SrO conversion and kinetics, strongly depends on the operating conditions (operating temperature and pressure strongly affects the thermodynamics and kinetics of the carbonation reaction), the kinetic study has been carried at operating conditions relevant for TCES-CSP applications, i.e. involving carbonation under high CO_2 partial pressure (1 atm) and at high temperature (900 °C – 1050 °C). Accordingly, the novelty of the present work consists in

modelling the kinetics of an Al_2O_3-stabilized composite with two different kinetic models, depending on the stage of the reaction, i.e. either the kinetically or diffusion controlled stage, have been used to fit the experimental conversion data. Therefore, the reaction rate, activation energy and the characteristic product layer thickness have been evaluated. Finally, comparison of the calculated conversion-time profiles, obtained from the applied kinetic models, with experimental data revealed a good agreement.

2. Experimental

2.1 Materials

The Al_2O_3-stabilized SrO granules have been prepared according to the procedure described in [30]. In particular, a $SrCO_3$ particles (Aldrich 472018, purity >99.9%) have been mixed with Al_2O_3 particles (MARTOXID KMS-96, purity 96,0%), used to inhibit the sintering/agglomeration phenomena, with a SrO-Al_2O_3 weight ratio of 66%/34%, in deionized water. Then, the obtained mixture has been calcined in a muffle furnace at 1000 °C for 3 hours. The calcined material has been gently crushed and sieved in the particle size range 200 - 600 μm.

Both the fresh and cycled SrO-Al_2O_3 composite samples have been subjected to different characterization analyses. Open pore-size distribution in the range of 0.0058−100 μm has been determined by mercury intrusion porosimetry (MIP; ThermoFinnigan 240). BET specific surface area measurements have been performed by N_2 gas adsorption (Flow Sorb II 2300, Micromeritics). Morphological and microstructural characterization has been carried out by scanning electron microscopy (Philips XL30 SEM-EDS for the fresh samples; FE-SEM-Zeiss SIGMA, Carl Zeiss GmbH, Germany for the cycled samples). Qualitative crystallographic analysis has been performed by X-ray diffractometry (XRD; Bruker D8 Advance powder diffractom- eter with Cu Kα radiation)

Details on the chemico-physical and morphological characterization of both SrO and the SrO-Al_2O_3 composite can be found in [30]. In brief, the morphological analysis, has shown that SrO (Fig. 2a) is

made of irregularly-shaped grains smaller than 10 μm, and that the SrO-Al_2O_3 composite (Fig. 2b) is characterized by a finer microstructure.

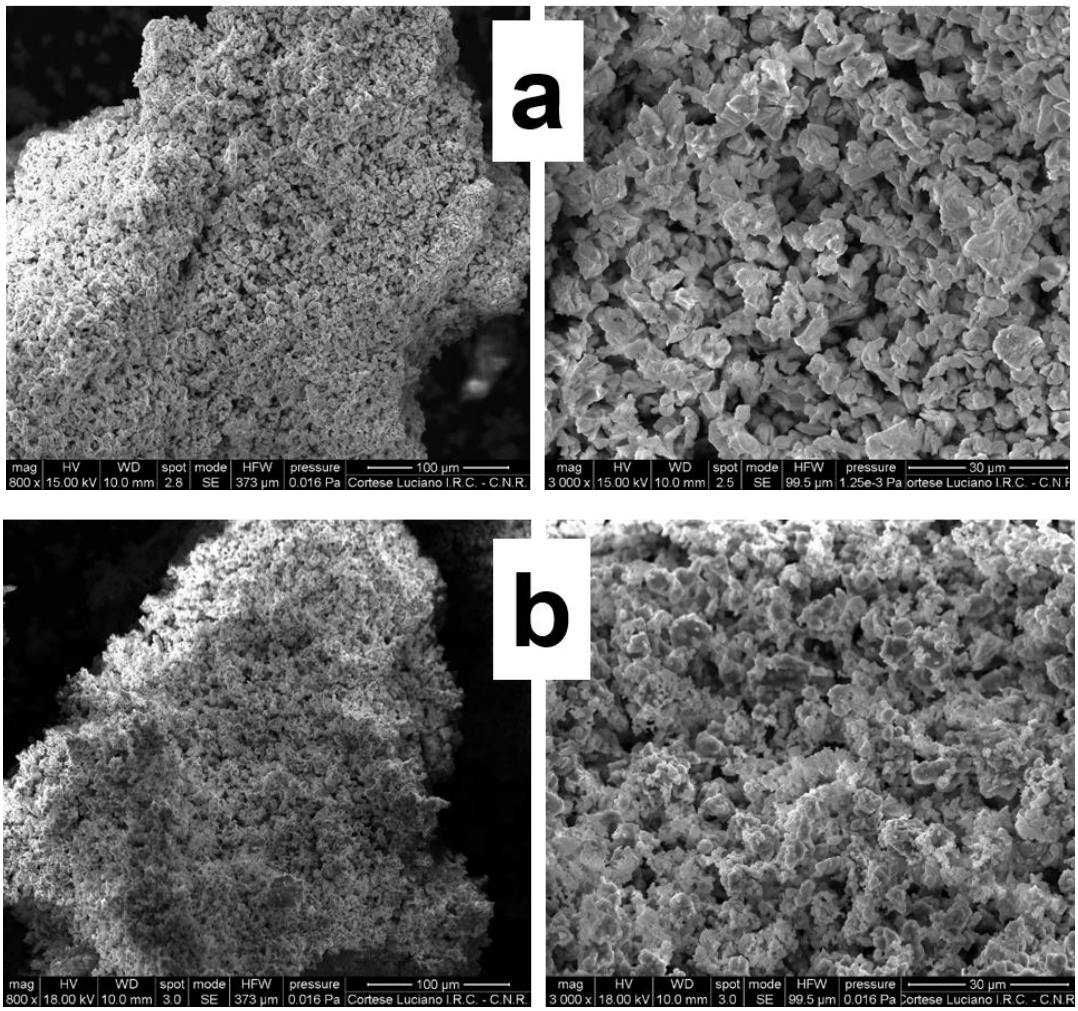

Fig. 2. SEM images at different magnification of fresh SrO (a) and SrO-Al_2O_3 composite (b) samples.

Then, from the surface analysis it has been obtained that both the raw SrO (0.52 m^2 g^{-1}) and the SrO-Al_2O_3 composite (1.26 m^2 g^{-1}) are characterized by low BET surface area, even though the presence of Al_2O_3 in the composite slightly increases the BET surface are due to a spacing effect [30].

As regards the XRD analysis, it was reported that the fresh SrO shows $SrCO_3$ reflections besides SrO peaks, since the material is prone to catch CO_2 from air during the specimen preparation and analysis [30]. The XRD analysis of the fresh composite SrO-Al_2O_3 sample shows the formation of strontium aluminates with different Sr/Al molar ratio: $Sr_3Al_2O_6$ with Sr/Al = 1.5, $SrAl_2O_4$ with Sr/Al = 0.5 [30].

2.2 Experimental apparatus and procedure

Carbonation/calcination cycles have been carried out in a STA 449 Jupiter (Netzsch Geraetebau, Selb, Germany) thermo-balance. The sample (35-45 mg) is initially heated at 30 °C/min in an inert atmosphere (Ar) up to the desired reaction temperature. Then, calcination and carbonation steps (with a duration time ranging from 30 to 60min, in order to obtain a stable value of carbonation conversion depending on the tested temperature) have been alternatively performed flowing (40 ml min^{-1} STP) either Ar or CO_2 gas, respectively, at atmospheric pressure.

In particular, five cycles (i.e. a number of cycles sufficient to reach stable carbonation performance [30]) in alternating atmospheres of CO_2 (P_{CO_2} = 1 atm) and Ar (P_{CO_2} = 0 atm) have been performed at four different temperatures (900, 950, 1000, 1025 and 1050°C). Then, the experimental data of the last cycle have been used to perform the kinetic study.

The SrO carbonation conversion, X, has been calculated from the sample mass variation:

$$X_{SrO} = \frac{\Delta m}{w\, m_i} \frac{M_{SrO}}{M_{CO_2}} \quad (3)$$

where Δm is the mass variation of the sample during the i-th carbonation, m_i is the mass of sample at the beginning of the i-th carbonation, w is the mass fraction of SrO in the sample, and M_{SrO} and M_{CO_2} are the molecular weights of SrO and CO_2, respectively.

2.3 Kinetic analysis

The heterogeneous carbonation reaction leads to the transformation of a solid (the metal oxide) and a gas (CO_2) into another solid (the carbonate) [42]. The reaction rate is expressed as the variation of the conversion degree with time, X(t). Indeed, varying with the time evolution of the reaction, X(t) can be characterized by distinctive shapes [42]. The aim of the kinetic analysis is, then, to analyze these shapes and link them to the specific fundamental mechanisms [42]. Considering that a reaction may be incomplete, namely X(t) typically does not reach unity, the extent of conversion, α, is commonly used in the analysis of solid-gas reaction kinetics. In particular, α ($0 < \alpha < 1$) is evaluated as:

$$\alpha = \frac{X}{X_u} \quad (4)$$

being X_u the ultimate carbonation conversion, i.e. a conversion limit at which no more significant conversion is observed (as the carbonation proceeds, the rate of the reaction decreases due to the formation of the carbonate product layer hindering the access of CO_2 molecules to the residual SrO, which leads to an ultimate conversion smaller than 100%). More specifically, two conversion limits, X_{u1} and X_{u2}, can be evaluated for the fast and slow stages of the carbonation reaction, respectively. X_{u1} is the carbonation conversion of the sorbent at the end of the fast kinetically controlled stage, whereas, X_{u2} is the carbonation conversion globally achieved at the end of the carbonation reaction. Therefore, the reaction rate ($d\alpha/dt$) of a gas-solid reaction is commonly described by the equation:

$$\frac{d\alpha}{dt} = r(T)f(\alpha) \quad (5)$$

where r(T) (min^{-1}) is the temperature-dependent reaction rate and $f(\alpha)$ is the reaction model describing the reaction mechanism. By integrating Eq. 5, the integral form of the kinetic model $g(\alpha)$ can be obtained:

$$g(\alpha) = \int_0^t \frac{d\alpha(t)}{f(\alpha)} \quad (6)$$

Once the time evolution of the extent of carbonation is known, α(t), the kinetic analysis can be performed by selecting a proper apparent kinetic model to fit the experimental data [42,43]. The main characteristic of these models is that all the mass transfer resistances, such as external diffusion, pore diffusion, and surface reaction, are lumped together [33,42]. The standard procedure is, then, to fit the experimental data with the selected kinetic model aiming at calculating an apparent global kinetic rate [33,42]. These kinetic rates obviously are not the same as the intrinsic reaction rate, which will depend on several experimental variables and/or morphological properties (e.g. particle size, specific surface area, etc.) [33,42]. Of course, the advantage of using apparent kinetic models is the simplicity, i.e. one expression can account for all the steps in a reaction. But at the same time, these models are scale-dependent due to the effect of transport phenomena [33,42].

Based on mechanistic assumptions, models are divided into nucleation, geometrical contraction, diffusion, or reaction-order [42]. In this work two different models have been applied to study the kinetics of the fast and slow stage of the SrO carbonation reaction.

For the fast carbonation stage (stage 1), the contracting sphere model has been used, which mainly assumes that nucleation occurs rapidly on the surface of the crystal and the rate is controlled by the resulting reaction interface progress towards the center of the crystal [42,43]. The mathematical expression in differential and integral form is [42,43]:

$$\frac{d\alpha}{dt} = r_1 3(1-\alpha)^{2/3} \quad (7)$$

$$1-(1-\alpha)^{1/3} = r_1 t \quad (8)$$

where r_1 (min^{-1}) is the apparent (i.e. depending on several material properties, such as particle size and specific surface area [42,44]) rate constant of the fast carbonation stage.

For the slow carbonation stage (stage 2), which is known to be controlled by the diffusion of the CO_2 molecules through the product layer, the Jander's three-dimensional diffusional model [42,43] has been used. Its main assumption is that the rate of carbonate formation decreases proportionally with the thickness of the product layer [42,43]. The mathematical expression in differential and integral form is [42,43]:

$$\frac{d\alpha}{dt} = r_2 \left[3(1-\alpha)^{2/3}\right] / \left[2\left(1-(1-\alpha)^{1/3}\right)\right] \quad (9)$$

$$(1-(1-\alpha)^{1/3})^2 = r_2 t \quad (10)$$

where r_2 (min^{-1}) is the rate constant of the slow carbonation stage.

Then, the reaction rates of the two carbonation stages, r_1 and r_2, have been evaluated by considering the logarithmic form of Eq. 8 and Eq. 10:

$$\ln[1-(1-\alpha)^{1/3}] = \frac{1}{n}\ln(r) + \frac{1}{n}\ln(t) \quad (11)$$

where n is either 1 or 2 depending on the stage of the carbonation reaction, i.e. fast or slow. Clearly, $\ln[1-(1-\alpha)^{1/3}]$ and ln(t) are linearly dependent, and the slope of this line is 1/n. More specifically, considering that the carbonation reaction is characterized by a double stage, a bi-linear plot should be

obtained, with slopes equal to 1 in the kinetically controlled stage and 1/2 in the diffusion controlled stage. Then, r_1 and r_2 are evaluated from the intercept of the plot.

The fitting quality of the used kinetic models to the experimental data has been assessed by evaluating the coefficient of correlation, R^2, changing between 0 to 1, and the HYBRID error function [45], where the lower the HYBRID value the better the fitting quality is. In particular, it is defined as:

$$HYBRID(\%) = \frac{100}{n-p}\sum_{i=1}^{i=n}\left[\frac{\left(X_{mod_i}-X_{exp_i}\right)^2}{X_{exp_i}}\right] \quad (12)$$

where X_{exp} and X_{mod} are the experimental and modeled carbonation conversion degree, respectively, n is the number of experimental points and p is the number of parameters of the equation.

According to several works available in the literature [41,46–49], the conversion, X_{u1}, at which the transition between the kinetically-controlled (stage 1) and diffusion-controlled periods (stage 2) takes place must also be related to the product layer thickness. Therefore, the changes observed in X_{u1} with the carbonation temperature have been explained referring to the changes in the product layer thickness with the carbonation temperature. Indeed, X_{u1} can be regarded as the critical SrO conversion corresponding to the critical product layer thickness [41]. In particular, according to Alvarez and Abanades [41], the thickness of the product layer at the end of the fast carbonation stage, h, can be calculated from X_{u1} as:

$$h = \frac{X_{u1}}{S_0}\frac{V_{SrCO_3}^M}{M_{SrO}} \quad (13)$$

where S_0 is the sorbent surface area per unit of mass, $V_{SrCO_3}^M$ is the molar volume of $SrCO_3$ and M_{SrO} is the molecular weight of SrO.

In order to evaluate the intrinsic reaction rate constant (k_s) of the carbonation reaction in the kinetically controlled stage, which is an intrinsic property of the material, the grain model has been applied, as proposed by Sun et al. [37]. This model assumes that: i) at the beginning of the reaction, stage 1, the diffusion resistance is negligible and the rate of reaction is high; hence, the chemical kinetics controls the reaction [37]; ii) the constant value of r_1 in the kinetic-controlled region obtained

from the slope of the linear plot, as described above, can also be extended to represent the true rate at the zero conversion point (i.e. $r_1 = r_0$) [37].

The specific rate at the beginning of the reaction can be written in power low as [37]:

$$\left.\frac{dX}{dt}\right|_{t=0} = 3r_1 = M_{SrO} k_s \left(P_{CO_2} - P_{CO_2}^{eq}\right)^n S_0 \quad (14)$$

where k_s is the intrinsic chemical reaction rate constant and $\left(P_{CO_2} - P_{CO_2}^{eq}\right)$ is the reaction driving force, i.e. the difference between the equilibrium and partial pressure of CO_2, n is the reaction order. k_s can be expressed according to Arrhenius equation:

$$k_s = k_0 exp\left(E/_{RT}\right) \quad (15)$$

being E the activation energy and k_0 the pre-exponential factor.

Sun et al. [37] determined that for CO_2 partial pressures driving force sufficiently high, i.e. ($P_{CO_2} - P_{CO_2}^{eq}$) >10 kPa, the reaction is zero-order (n = 0). In this work, all the experiments have been carried at a CO_2 partial pressure equal to 1 atm; therefore, the reaction order can be always assumed equal to zero and, considering Eq. (15), Eq. (14) can be re-written in logarithmic form as:

$$\ln(r_1) = ln(M_{SrO} k_0 S_0/3) - E/_{RT} \quad (16)$$

Therefore, the two parameters, E and k_0 can be obtained by fitting Eq. (16) with the values of the apparent kinetic rates, r_1, evaluated at the different investigated temperatures.

3. Results and discussion

3.1 Materials characterization

Compared to the fresh SrO-Al_2O_3 composite, the BET surface area of the cycled composite samples is always increased at all the tested working temperatures, but reaching the maximum value (1.90 m^2 g^{-1}) after cycling at 1000°C (Table 1).

Looking at the MIP results for the samples cycled at 900, 1000 and 1050 °C (Table 1 and Fig. S1), the total pore volume decreases for all the composite samples after cycling compared to the uncycled material (477 mm^3 g^{-1}). The general pore volume decrease can be imputed to a disappearance of pores

due to thermal contraction; a higher relative contribution of small pores can be observed for the sample cycled at 1000°C, which results in the lowest values of average diameters (Table 1 and Fig. S1). Based on the MIP graphs the percentage of contribution of pores smaller than 1 μm are 13.5%, 14.3% and 11.2% for samples cycled at 900, 1000 and 1050°C respectively. Focusing on pores with dimension lower than 100 nm, values of 6.1%, 7.1% and 3.7% have been found for the same samples respectively.

Table 1. Results of BET specific surface area ($m^2 g^{-1}$) and MIP analysis of the fresh and cycled $SrO\text{-}Al_2O_3$ composite samples.

Sample	BET $m^2 g^{-1}$	Total intruded volume $mm^3 g^{-1}$	Average pore μm	Density $g cm^{-3}$
Fresh	1.26	477	0.89	1.13
900 °C	1.73	405	0.33	1.00
1000 °C	1.90	424	0.20	0.90
1050 °C	1.40	400	0.44	0.95

The SEM microstructure images (Fig. 3) are in accordance with the porosity results, showing at lower magnification a slight compaction trend of the material at increasing temperature. A diffused microporosity affecting the skeleton material has been particularly observed in the sample cycled at 1000°C. At 1050°C the pores network is less evident while voids more similar to microcracks appear within a more compact microstructure, where grains are more defined.

The microstructure features reflect on the XRD spectra (Fig. S2) aspect. The spectrum of the sample cycled at 1050°C shows more defined signals which are clearly typical of a material with higher crystalline character. No important differences have been found concerning the crystallographic composition: mixed Sr-Al oxides and hydroxide have been found besides strontianite and alumina.

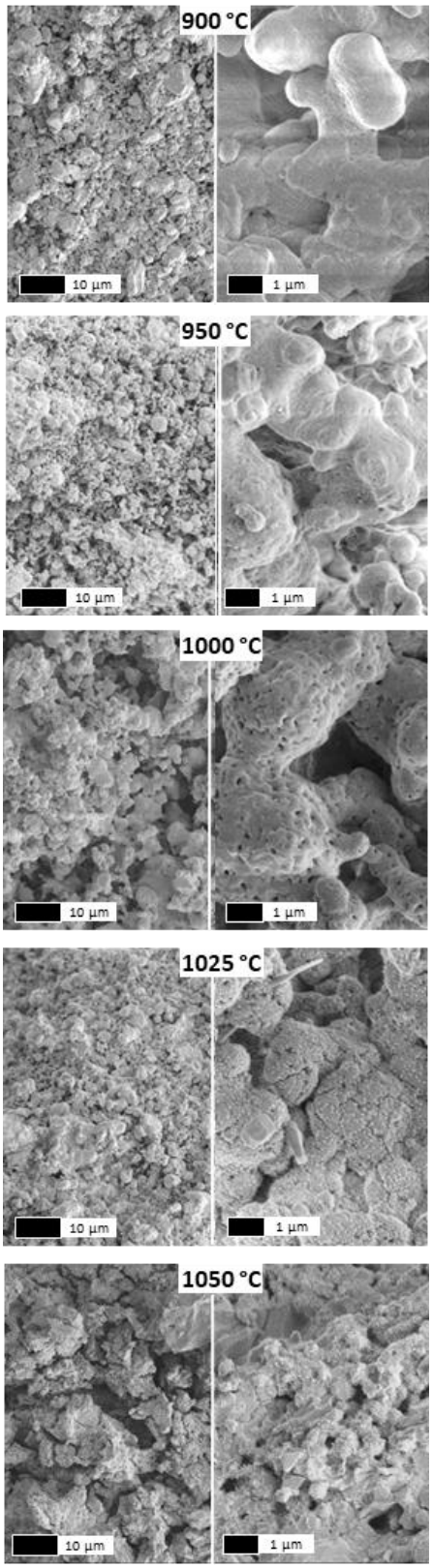

Fig. 3. FE-SEM images, at different magnifications, of the SrO-Al_2O_3 composite samples cycled at the different investigated temperatures.

The material cycled at 1000 °C shows the presence of strontianite and of the mixed hydroxide but a limited amount of the mixed oxide with high Sr/Al ratio ($Sr_3Al_2O_6$) that becomes even more evident at the higher temperatures. Such an evolution of the relative amount of the mixed phases can be proposed, but due to overlapping peaks and unknown scattering factors, more investigations are needed for quantification purposes, which are however out of the scope of this paper.

The bulk density of the sample cycled at 1000°C is lower compared to the other two samples. However, these values could be affected by the changes of the relative content of crystallographic phases formed at the different temperatures, as appears from XRD patterns (Fig. S3).

3.2 Kinetic analysis

The results of thermo-gravimetric tests performed on the SrO-Al_2O_3 composite at different temperatures are shown in Fig. 4 and Fig. S3. It is clear that the experimentally detected calcination goes always to completion, as highlighted by the signal achieving the baseline. With reference to the carbonation step, the sample is characterized by an increased carbonation conversion with increasing number of cycle, according to the results reported in [30]. A thorough investigation of the carbonation/calcination performances of the SrO-Al_2O_3 composite as affected by increasing number of cycles can be found in our previous work [30]. However, a brief overview of the main results there reported on the SrO-Al_2O_3 multicyclic behavior is also provided hereafter, for the sake of clarity.

In brief, Ammendola et al. [30] showed that the SrO-Al_2O_3 composite behavior becomes repeatable after 4-5 carbonation/calcination cycles (i.e. the carbonation performances obtained for the 5^{th} cycle are representative of the residual carbonation performances of the composite). More specifically, this initial increase in the carbonation conversion has been explained on the basis of the fact that the evolution of the sorbent during cyclic operations is affected by of two opposed phenomena, sintering and self-reactivation; the carbonation reactivity is either decreased or increased with cycling depending on the prevalence of one over the other [50–52]. Indeed, from one hand, it has been shown that the composite is naturally affected by sintering phenomena, as also highlighted in the SEM

analysis performed in the present work at the different investigated temperature (Fig. 3), which would hinder its multicyclic performances/reactivity [30].

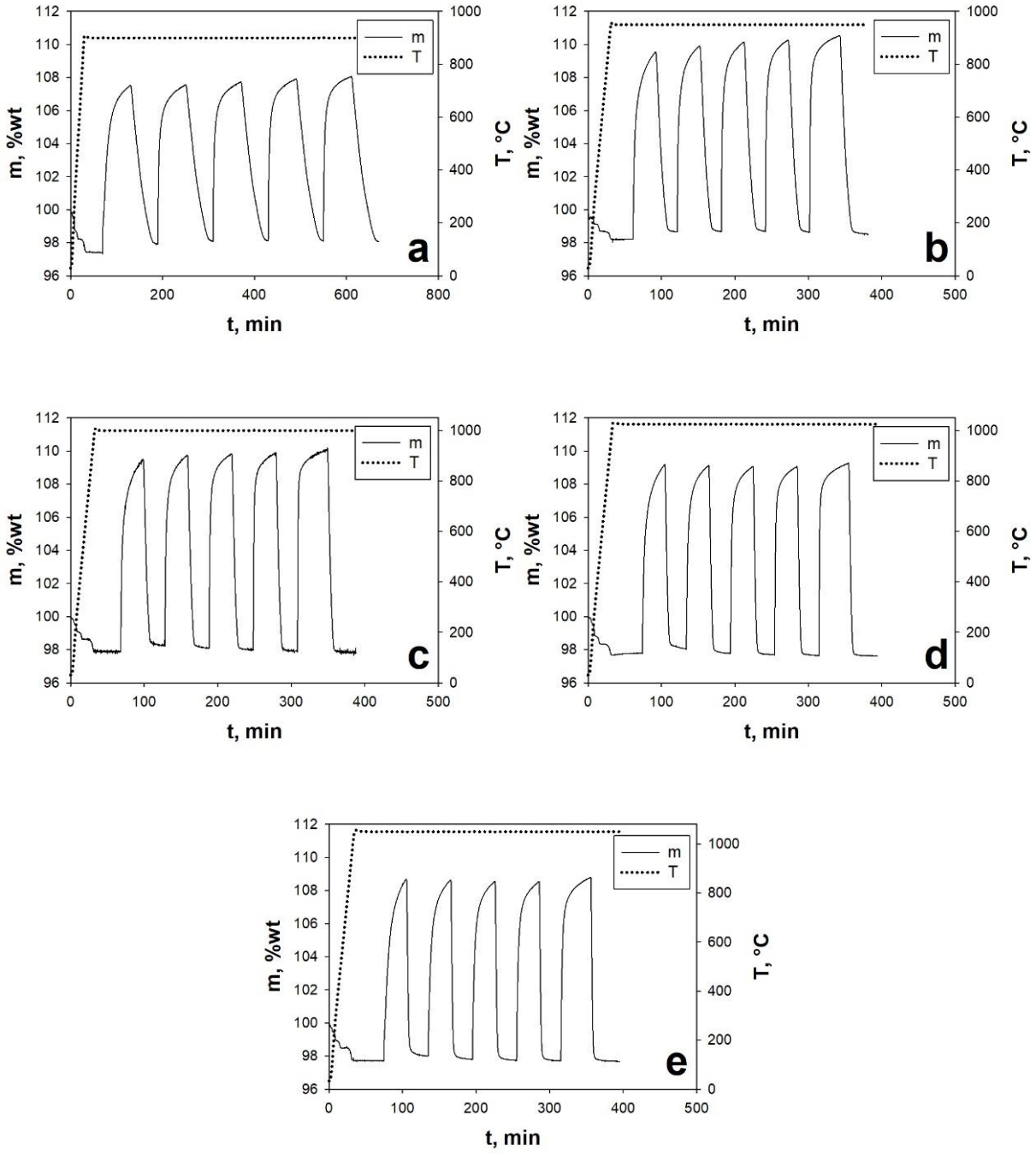

Fig. 4. TGA cycles of the SrO-Al_2O_3 composite at different temperatures: (a) 900, (b) 950, (c) 1000, (d) 1025, (e) 1050 °C. Carbonation and calcination performed respectively in CO_2 and Ar atmosphere.

However, it has been also shown that the SrO-Al_2O_3 composite is characterized by limited sintering phenomena, i.e. just negligible morphological modifications, with respect to the raw SrO, which is characterized by severe morphological changes [30]. In particular, it has been reported that the distribution of Al_2O_3 and SrO remains homogenous after the cycles, which means that the initial structure, capable of inhibiting the sintering, is kept stable over the cycles. Indeed, the observed increase in the sorbent reactivity during the first cycles has been explained by referring to the self-reactivation phenomena [27,53–56], i.e. the sample experiences an increase of BET specific surface area of about 50% after 4-5 cycles [30], as further confirmed in the present manuscript and discussed in the previous paragraph. It has been explained that the combination of the increased BET specific surface area with the limited sintering phenomena (due to the presence of inhibitor), leads to an increase of the amount of SrO available to the carbonation reaction, which explains the initial enhancement of the carbonation performances (Fig. 4) [30].

Fig. 5a reports the experimental values of the carbonation conversion degree (X) of the last carbonation cycle obtained at the different investigated temperatures, according to Eq. (3). It can be clearly observed that the rate of carbonation changes with the conversion degree in the course of the reaction, i.e. the reaction is under kinetic control at very lower conversion levels (stage 1), whereas it is diffusion controlled at higher conversion levels (stage 2).

More specifically, the reaction rate is fast at low conversion levels, with the different initial rates strongly depending on temperature. Then, as the carbonation reaction proceeds and the conversion increases, the slope of the conversion-time profile decreases and, therefore, the reaction rate decreases, due to thickening of the product layer around each pore; then, when the conversion gets close to an ultimate conversion, X_u, at which no more significant conversion is attained at each temperature, the rate of carbonation approaches to zero. In other words, the dense $SrCO_3$ forming on the pore wall prevents CO_2 diffusion through it. Thus, the reaction tends to be diffusion-controlled as it goes on. The strong dependence of the carbonation rate on the temperature has been more clearly

shown by polishing the plots form the effect of X_u (which is itself depending on the temperature), i.e. by plotting the extent of carbonation (α) (Fig. 5b).

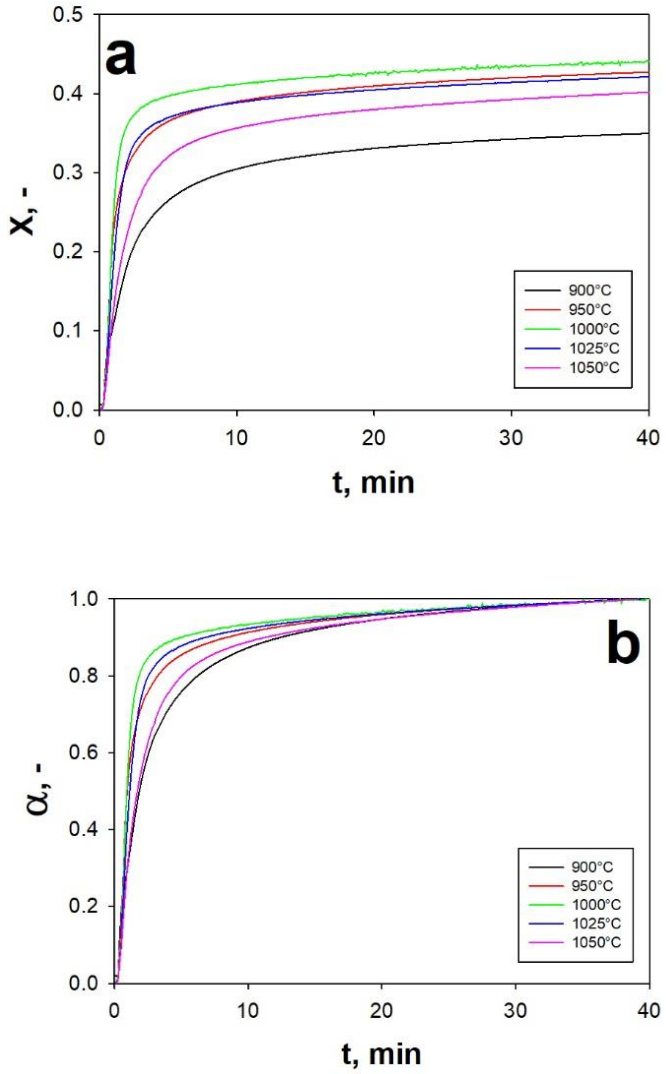

Fig. 5. Experimental carbonation conversion degree (X) (a) and carbonation extent (α) (b) as functions of time obtained for the SrO-Al_2O_3 composite at different temperatures.

Fig. 6 shows the graphical representation of the kinetic model (Eq. (11)), i.e. the plots of the experimental values of $\ln[1 - (1 - \alpha)^{1/3}]$ vs $\ln(t)$ for different temperatures. Here, the two different linear segments of the plots clearly evidence the existence of stage 1 and stage 2 of the carbonation reaction, having two different rate-controlling steps (i.e. kinetic control and diffusion through product-layer control).

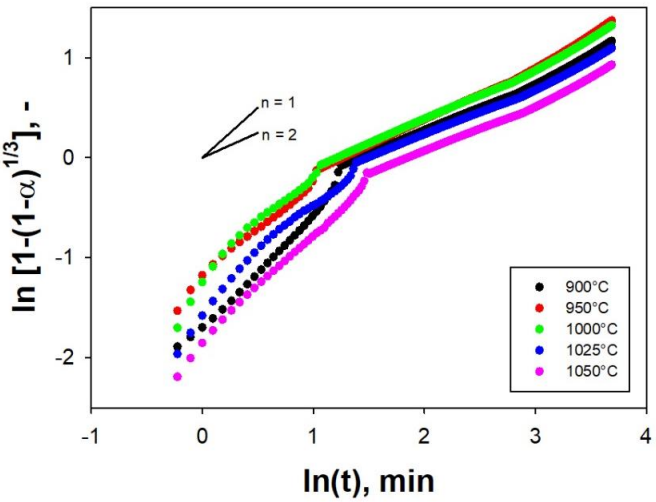

Fig. 6. Plots of ln[1 - (1 - α)$^{1/3}$] vs. ln(t) obtained for the SrO-Al_2O_3 composite at different temperatures.

From the analysis of Fig. 6, i.e. from the slope and intercept of the two linear segments of the plot, the kinetic parameters have been evaluated (Table 2). The SrO conversion degree at the end of stage 1 (X_{u1}) and stage 2 (X_{u2}) have been also evaluated from Fig. 6, namely X_{u1} has been evaluated as the carbonation conversion corresponding to the change of the slope and X_{u2} as carbonation conversion at the end of the end of the plot.

Table 2. Parameters of the apparent kinetic models and fitting comparison between the modeled and experimental data for the carbonation of the SrO-Al_2O_3 composite.

	Stage 1				Stage 2			
T	n_1	r_1 10^{-3}	R^2	HYB.	n_2	$r_2 10^{-4}$	R^2	HYB.
°C	-	s^{-1}	-	%	-	s^{-1}	-	%
900	0.939	3.418	0.994	0.196	0.490	4.307	0.981	0.201
950	1.049	4.725	0.989	0.198	0.540	7.444	0.969	0.199
1000	0.912	5.176	0.967	0.177	0.511	8.715	0.975	0.212
1025	0.860	4.212	0.981	0.181	0.476	9.977	0.967	0.191
1050	0.909	3.041	0.994	0.195	0.477	10.443	0.984	0.202

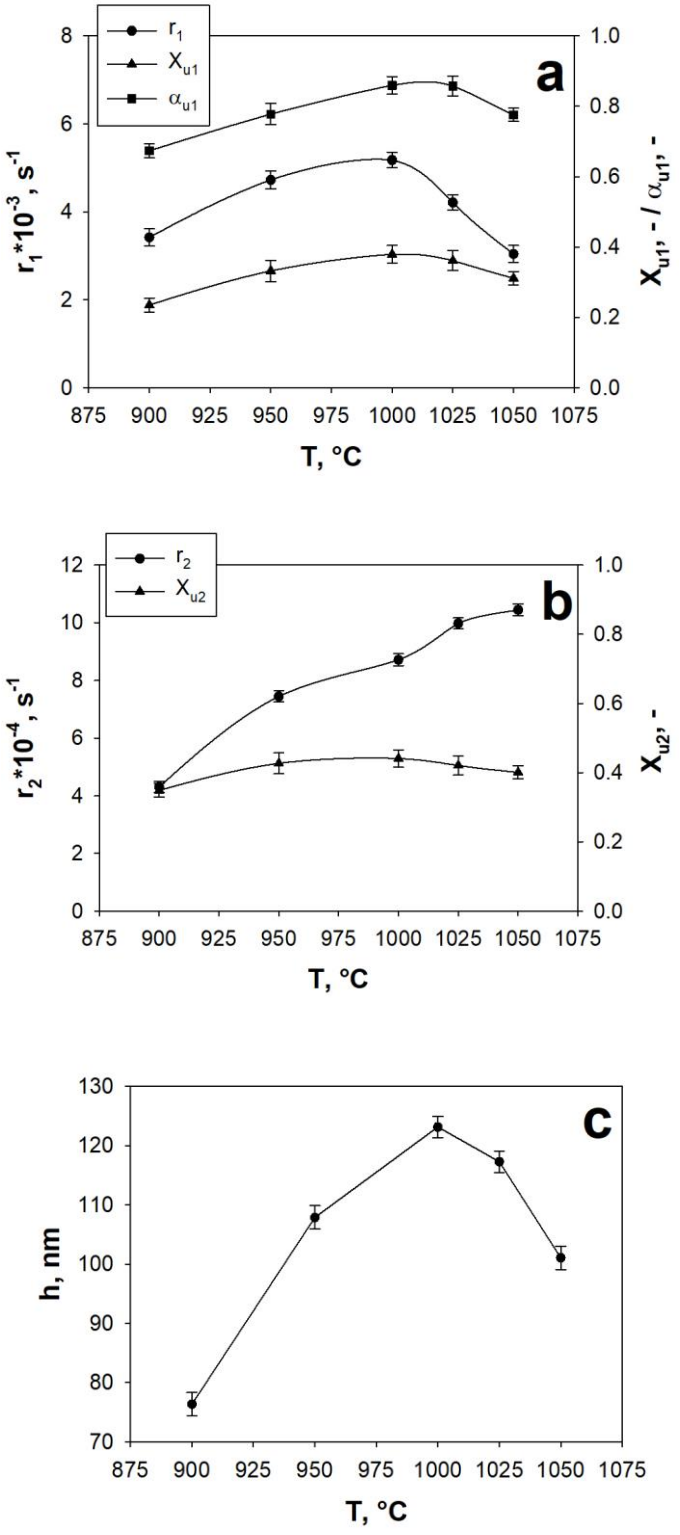

Fig. 7. Apparent kinetic rates (r), ultimate carbonation conversion degree (X_u) and carbonation extent (α_u) for the stage 1 (a) and stage 2 (b) (by definition $\alpha_{u2} = 1$, regardless of the carbonation temperature) of the carbonation reaction and thickness (h) of the $SrCO_3$ product layer (h) (c) obtained for the $SrO\text{-}Al_2O_3$ as functions of the temperature.

The results are reported in Table 1 and Fig. 7, where it is worth noting the different scales of y-axes for r_1 and r_2. As reported above, in ideal cases, the slopes of the fitted curves should be 1 ($1/n_1$) and 0.5 ($1/n_2$), for stage 1 (contraction volume model) and for stage 2 (Jander's model), respectively. Congruently, there is a good agreement of the experimental data with these theoretical values. Indeed, the slope for stage 1 ranges from 0.860 to 1.032 and from 0.490 to 0.540 for stage 2 (Table 1). Such slight deviations from the theoretical values are explainable because carbonation is a quite complex process occurring in multiple steps and the exact point where stage 1 finishes and stage 2 begins is hardly identified and a smooth transition is likely to occur in real cases [43].

Clearly, the analysis of Table 1 and Fig. 7a shows that the rate of the fast carbonation stage, r_1, is increased when temperature is increased from 900 to 1000 °C, which is in line with the reaction kinetics being typically enhanced by increasing temperatures. However, it can be also observed that the rate of the fast carbonation stage does not increase monotonically for temperatures larger than 1000 °C. Indeed, there is a temperature at which the rate of the fast carbonation stage (stage 1) reaches a maximum, above which it gradually decreases as the equilibrium temperature (1175 °C [23]) is approached. Therefore, the SrO-Al_2O_3 composite is characterized by optimal performances, in terms of kinetics of the fast carbonation reaction stage, at 1000 °C. These evidences are in agreement with the results obtained from the BET, MIP and SEM analyses; indeed, the improved reactivity of the composite with increasing the temperature from 900 to 1000 °C can be ascribed to the enhanced self-reactivation phenomenon, as highlighted by the increased BET surface area (Table 1) and by the improved microporosity (Fig S1 and Fig. 3). Moreover, according to thermodynamics and as clearly inferable from Fig. 1, the carbonation reaction takes place when the P_{CO_2} is higher than the equilibrium partial pressure of CO_2 at a certain temperature, $P_{CO_2}^{eq}$. In particular, at a fixed P_{CO_2} (1 atm), $P_{CO_2}^{eq}$ increases with increasing temperatures (Eq. (2)), causing the decrease of the thermodynamic pressure driving force $\left(P_{CO_2} - P_{CO_2}^{eq}\right)$, i.e. the carbonation reaction tends to become thermodynamically unfavored, as typical of exothermic reactions [37,57–59]. This means that, as the temperature is

increased, at fixed P_{CO_2}, the initiation of the reverse reaction (calcination) becomes favored thermodynamically around the equilibrium temperature (1175 °C) [37,57–59].

This same trend has been reported by different authors [32,40,48] for the $CaO/CaCO_3$ system operated near equilibrium conditions. Obviously, the fact that, under operating conditions suitable for TCES-CSP applications, the fast carbonation rate does not monotonically increase with temperature is very important and the temperature at which the reaction rate is at its maximum is a key input for real applications. Indeed, from one hand, the plant efficiency will increase at higher carbonation temperature due to the higher power generation efficiency, according to the second law of thermodynamics and Carnot efficiency [32]. On the other hand, it should be considered that temperatures nearby equilibrium negatively affect the carbonation kinetics.

Likewise, from Fig. 7a it can be observed that the carbonation conversion achievable at the end of the stage 1, i.e. at the boundary between the fast reaction and solid-state diffusion stages, is also characterized by an optimum value at 1000 °C. Indeed, it increases with temperature up to 1000 °C, whereas it decreases for higher temperatures, which is in agreement with the reaction rate increasing up to 1000 °C and then decreasing for higher temperatures. This same trend is also obtained for the extent of carbonation, α, thus indicating that an increase of temperature up to 1000°C makes it possible to increase the percentage of solid converted in the fast carbonation stage, i.e. the contribution of the fast carbonation stage to the global carbonation conversion is enhanced. This result, i.e. the existence of a non-linear dependence on the temperature, has been also explained referring to the critical product layer thickness, namely the thickness of the carbonate layer formed on the free surfaces of SrO marking the end of the fast reaction stage (stage 1) [41], which reaches a maximum value at 1000 °C. The obtained values of the $SrCO_3$ product layer thickness, h, at the end of the fast carbonation stage are reported in Fig. 7c as a function of the temperature. Clearly, according to previous experimental evidences available for the $CaO/CaCO_3$ system even under substantially different operation conditions [41,46–49], an increase in the product layer thickness (from 76 to 123 nm) has been obtained with increasing the carbonation temperature in the range 900 – 1000 °C,

namely for temperatures sufficiently away from the equilibrium temperature (i.e. before the reaction rate is inverted because of the above-discussed thermodynamic limitations [37]). This result can be explained referring to a recent mechanistic kinetic study published by Li et al. [41] in which the authors investigated the effect of the reaction temperature on the carbonation reaction through atomic force microscopy, thus obtaining images of the CaO and $CaCO_3$ surfaces reacting with CO_2. Interestingly, they found that larger product islands are formed at higher carbonation temperatures, which was explained as a result of the faster diffusion of product molecules or ions at higher temperatures [41]. As a consequence, a larger product layer thickness is formed at higher temperatures, thus increasing the CO_2 carrying capacity of the CaO [41].

During the slow carbonation stage, on the contrary, the reaction rate monotonically increases with increasing temperatures (Fig. 7b), which is in line with the enhanced diffusional transport of CO_2 molecules within the carbonate layer at higher temperatures. From the analysis of Fig. 7b it can also be inferred that carbonation resulted in greater final conversion, X_{u2}, when temperature was increased up to 1000 °C. This result is in contrast to the thermodynamic principles involving that, the carbonation should achieve higher final conversion at lower temperatures, in line with the exothermic nature of the carbonation reaction and with the increased thermodynamic driving of the carbonation reaction $\left(P_{CO_2} - P_{CO_2}^{eq}\right)$ as the temperature moves away from the equilibrium temperature. In fact, even though in contrast to thermodynamic predictions, these observations agree well with previous works on CaO [34,36] and SrO [20] carbonation. Also this result can be explained by referring to the enhanced solid phase diffusional transport of CO_2 through the $SrCO_3$ product layer at higher temperatures. On the contrary, slower diffusion at lower temperature hinders the achievement of larger ultimate conversion within reasonable time frames [34,36]. Obviously a further increase of temperature is detrimental in terms of final conversion degree as thermodynamics constraints, deriving from the exothermicity of the carbonation reaction, predominate over the enhanced CO_2 diffusional mobility.

Then, the intrinsic rate constant (k_s) and its dependence on the temperature may be evaluated considering only the temperatures up to 1000 °C, i.e. before the inversion of the reaction rate caused by the above-mentioned thermodynamic limitations (where the forward reaction would presumably dominate) [37]. In particular, fitting the calculated data of reaction rate in the kinetically controlled stage (r_1) with Eq (15), the activation energy of the reaction, E, and the pre-exponential factor k_0 have been evaluated (Fig. 8).

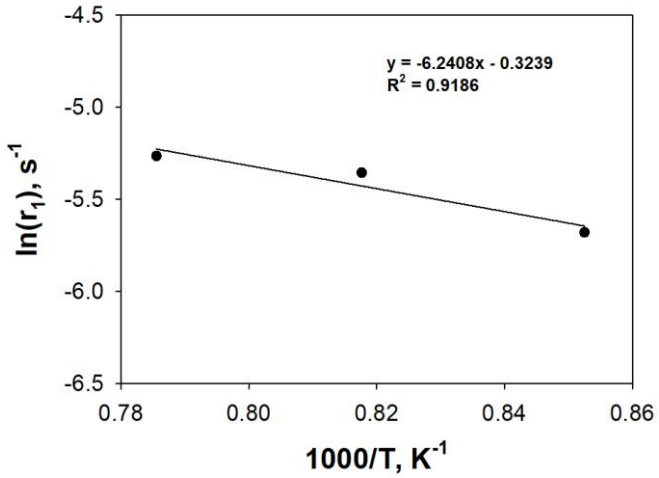

Fig. 8 ln (r_1) vs 1000/T (Eq. (15)) for the carbonation reaction of the composite SrO-Al_2O_3.

Thus, the temperature dependency of the intrinsic rate constant, k_s, in the operating temperature range of 900 - 1000 °C has been evaluated and expressed according to the following equation:

$$k_s = 1.679 \times 10^{-2} exp(-51.886/RT) \quad (16)$$

In particular, the obtained activation energy (E = 51.886 kJ mol^{-1}) for the carbonation reaction of the SrO-Al_2O_3 composite is very similar to the value reported in a recent work on the carbonation kinetics of pure SrO [20].

The apparent kinetic rates obtained in the stage 1 and stage 2 of the carbonation reaction have been used to evaluate the time evolution of the carbonation conversion in order to validate the obtained results. Fig. 9 shows the conversions predicted by the proposed model equations, i.e. employing the parameters obtained in the kinetic and diffusion control regimes, in comparison with the experimental curves. Clearly, neither of the two proposed models (the contracting volume model and Jander's model) is able to properly describe the entire carbonation reaction, i.e. over the entire time frame.

This evidence is due to the fact that there is always a transition zone, i.e. a time frame in which the carbonation reaction is controlled by both chemical reaction of the CO_2 molecules with the SrO surface and by the diffusion of CO_2 through the building up carbonate layer. However, although a single theoretical model is not able to capture all of the features and describe the whole carbonation reaction, it nevertheless provides a simplified basis for kinetics investigation [43]. Indeed, the proposed models can separately describe with a rather good accuracy the two stages of the carbonation reaction, as clearly evidenced by the good match between the experimental data of the stage 1 and stage 2 with the theoretical values predicted by the contracting volume model and Jander's model, respectively. Therefore, the combined prediction using the parameters obtained in both the two control regimes can give the best results in the entire range of conversion for the reported experimental data.

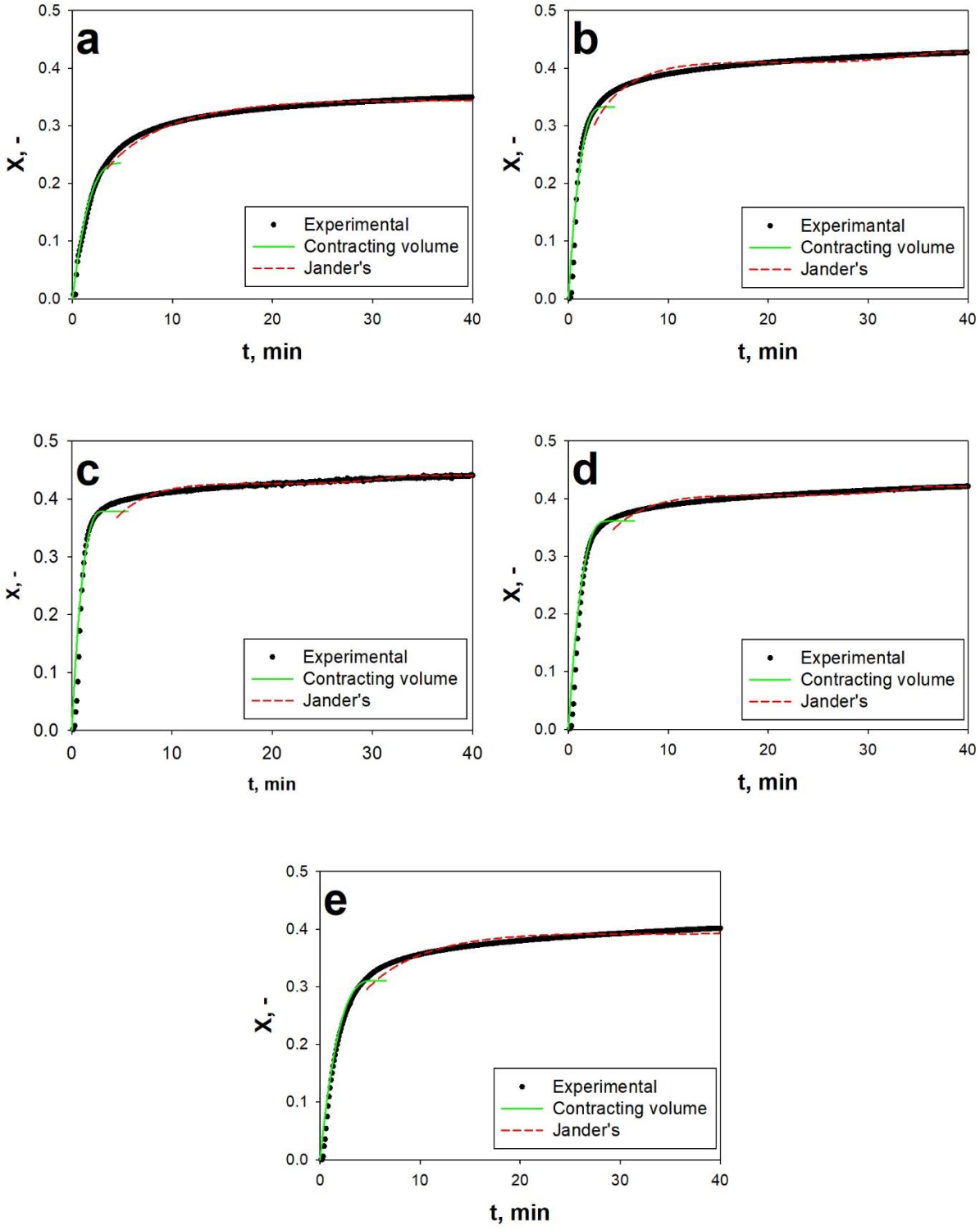

Fig. 9. Comparison between the experimental value of the conversion degree (X) and the theoretical values, predicted using the kinetic parameters obtained in the kinetic (contracting volume model) and diffusion (Jander's model) rate control regimes, for the SrO-Al_2O_3 composite. Carbonation temperature: (a) 900, (b) 950, (c) 1000, (d) 1025, (e) 1050 °C.

4. Conclusions

The carbonation kinetics of a SrO-Al_2O_3 composite (34%wt of Al_2O_3) has been investigated for thermochemical energy storage in CSP plants. Tests have been performed in a thermogravimetric analyzer at operating conditions relevant for TCES, namely at 1 atm of CO_2 partial pressure within the temperature range of 900 °C – 1050 °C.

The kinetics of the carbonation reaction from TG experiments has been analyzed by applying two different kinetic models (the contracting volume model and the Jander's model), depending on the reaction stage, in order to thus get useful information for design and optimization of the SrO carbonation reactor. Then, the reaction rate, activation energy and the characteristic product layer thickness have been evaluated.

The main conclusions and observations derived from the kinetic study are:

- The carbonation of SrO occurs in two distinct phases: i) a fast carbonation stage (stage 1) in which the carbonation rate is kinetically controlled by the chemical reaction of the CO_2 molecules with the fresh oxide surface; ii) a slow carbonation stage (stage 2) controlled by the diffusion of CO_2 through the carbonate layer.
- Neither of the two selected models (the contracting volume model and Jander's model) can suitably describe the carbonation reaction over the entire time frame since there is always a transition period in which the carbonation reaction is controlled by both chemical reaction and CO_2 diffusion through the building up carbonate layer. However, the two stages of the carbonation reaction can be separately described with quite good accuracy by the two proposed models, i.e. stage 1 by the contracting volume model and stage 2 by the and Jander's model.
- At operating conditions functional for TCES-CSP applications, the carbonation rate does not monotonically increase with the temperature. Indeed, it rapidly increases with increasing temperature from 900 to 1000 °C, whereas, above this temperature it decreases gradually as the

thermodynamic equilibrium temperature is approached, i.e. when the initiation of the reverse reaction (calcination) starts to become favored thermodynamically.

- The carbonation conversion achievable at the end of the stage 1, X_{u1}, i.e. at the transition between the fast reaction and solid-state diffusion stages, also increases with temperature up to 1000 °C, whereas it decreases for higher temperatures, which is in agreement with the reaction rate increasing up to 1000 °C and then decreasing for higher temperatures. This result has been also linked to the critical carbonate product layer, h, at the end of the fast carbonation stage, which has been found to increase (from 76 to 123 nm) with increasing the carbonation temperature in the range 900 – 1000 °C, namely for temperatures sufficiently away from the equilibrium temperature.
- In spite of thermodynamics predicting lower conversions with increasing temperatures due to the exothermic character of the carbonation reaction (i.e. exothermic reactions are thermodynamically unfavoured at higher temperatures), the ultimate carbonation conversion has been found to increase when the temperature is increased from 900 up to 1000 °C, due to solid phase diffusional transport of CO_2 through the $SrCO_3$ product layer becoming more efficient at higher temperatures. On the contrary, temperatures higher than 1000 °C have been found to lead to a decrease of the final conversion degree as the enhanced CO_2 diffusional mobility is outbalanced by the thermodynamics limitations, involving the hindrance of the exothermic reactions as the temperature is increased.
- The intrinsic carbonation kinetic constant and its dependence on the temperature has been also evaluated in the temperature range 900 – 1000 °C; the activation energy has been found to be 52 kJ mol^{-1}.

Aknowledgements

Mr. Luciano Cortese is gratefully acknowledged for SEM analyses and Dr. Elettra Papa for BET and MIP measurements.

References

[1] P. Salatino, P. Ammendola, P. Bareschino, R. Chirone, R. Solimene, Improving the thermal performance of fluidized beds for concentrated solar power and thermal energy storage, Powder Technol. 290 (2016) 97–101. doi:10.1016/j.powtec.2015.07.036.

[2] C. Prieto, P. Cooper, A.I. Fernández, L.F. Cabeza, Review of technology: Thermochemical energy storage for concentrated solar power plants, Renew. Sustain. Energy Rev. 60 (2016) 909–929. doi:10.1016/J.RSER.2015.12.364.

[3] X. Chen, Z. Zhang, C. Qi, X. Ling, H. Peng, State of the art on the high-temperature thermochemical energy storage systems, Energy Convers. Manag. 177 (2018) 792–815. doi:10.1016/j.enconman.2018.10.011.

[4] L. André, S. Abanades, Evaluation and performances comparison of calcium, strontium and barium carbonates during calcination/carbonation reactions for solar thermochemical energy storage, J. Energy Storage. 13 (2017) 193–205. doi:10.1016/j.est.2017.07.014.

[5] H. Zhang, J. Baeyens, G. Cáceres, J. Degrève, Y. Lv, Thermal energy storage: Recent developments and practical aspects, Prog. Energy Combust. Sci. 53 (2016) 1–40. doi:10.1016/J.PECS.2015.10.003.

[6] G. Alva, L. Liu, X. Huang, G. Fang, Thermal energy storage materials and systems for solar energy applications, Renew. Sustain. Energy Rev. 68 (2017) 693–706. doi:10.1016/J.RSER.2016.10.021.

[7] G. Alva, Y. Lin, G. Fang, An overview of thermal energy storage systems, Energy. 144 (2018) 341–378. doi:10.1016/J.ENERGY.2017.12.037.

[8] J. Lizana, R. Chacartegui, A. Barrios-Padura, J.M. Valverde, Advances in thermal energy storage materials and their applications towards zero energy buildings: A critical review, Appl. Energy. 203 (2017) 219–239. doi:10.1016/j.apenergy.2017.06.008.

[9] C. Ortiz, J.M. Valverde, R. Chacartegui, L.A. Perez-Maqueda, P. Giménez, The Calcium-Looping (CaCO3/CaO) process for thermochemical energy storage in Concentrating Solar Power plants, Renew. Sustain. Energy Rev. 113 (2019) 109252. doi:10.1016/j.rser.2019.109252.

[10] S.E.B. Edwards, V. Materić, Calcium looping in solar power generation plants, Sol. Energy. 86 (2012) 2494–2503. doi:10.1016/j.solener.2012.05.019.

[11] J.M. Valverde, F. Raganati, M. a. S. Quintanilla, J.M.P. Ebri, P. Ammendola, R. Chirone, Enhancement of CO2 capture at Ca-looping conditions by high-intensity acoustic fields, Appl. Energy. 111 (2013) 538–549. doi:10.1016/j.apenergy.2013.05.012.

[12] F. Raganati, P. Ammendola, Sound-Assisted Fluidization for Temperature Swing Adsorption and Calcium Looping: A Review, Materials (Basel). 14 (2021) 672. doi:10.3390/ma14030672.

[13] F. Raganati, R. Chirone, P. Ammendola, Preliminary Study on Sound Assisted Calcium Looping for TCES in CSP Applications, Chem. Eng. Trans. 74 (2019) 427–432. doi:10.3303/CET1974072.

[14] F. Raganati, R. Chirone, P. Ammendola, Calcium-looping for thermochemical energy storage in concentrating solar power applications: Evaluation of the effect of acoustic perturbation on the fluidized bed carbonation, Chem. Eng. J. 392 (2020) 123658. doi:10.1016/j.cej.2019.123658.

[15] J.A. Almendros-Ibáñez, M. Fernández-Torrijos, M. Díaz-Heras, J.F. Belmonte, C. Sobrino, A review of solar thermal energy storage in beds of particles: Packed and fluidized beds, Sol. Energy. 192 (2019) 193–237. doi:10.1016/j.solener.2018.05.047.

[16] S. Flegkas, F. Birkelbach, F. Winter, N. Freiberger, A. Werner, Fluidized bed reactors for solid-gas thermochemical energy storage concepts - Modelling and process limitations,

Energy. 143 (2018) 615–623. doi:10.1016/j.energy.2017.11.065.

[17] A. Solé, I. Martorell, L.F. Cabeza, State of the art on gas–solid thermochemical energy storage systems and reactors for building applications, Renew. Sustain. Energy Rev. 47 (2015) 386–398. doi:10.1016/j.rser.2015.03.077.

[18] M. Angerer, M. Becker, S. Härzschel, K. Kröper, S. Gleis, A. Vandersickel, H. Spliethoff, Design of a MW-scale thermo-chemical energy storage reactor, Energy Reports. 4 (2018) 507–519. doi:10.1016/j.egyr.2018.07.005.

[19] A. Alovisio, R. Chacartegui, C. Ortiz, J.M. Valverde, V. Verda, Optimizing the CSP-Calcium Looping integration for Thermochemical Energy Storage, Energy Convers. Manag. 136 (2017) 85–98. doi:10.1016/j.enconman.2016.12.093.

[20] S. Zare Ghorbaei, H. Ale Ebrahim, Carbonation reaction of strontium oxide for thermochemical energy storage and CO2 removal applications: Kinetic study and reactor performance prediction, Appl. Energy. 277 (2020) 115604. doi:10.1016/j.apenergy.2020.115604.

[21] R. Chacartegui, A. Alovisio, C. Ortiz, J.M. Valverde, V. Verda, J.A. Becerra, Thermochemical energy storage of concentrated solar power by integration of the calcium looping process and a CO 2 power cycle, Appl. Energy. 173 (2016) 589–605. doi:10.1016/j.apenergy.2016.04.053.

[22] L. Meroueh, K. Yenduru, A. Dasgupta, D. Jiang, N. AuYeung, Energy storage based on SrCO3 and Sorbents—A probabilistic analysis towards realizing solar thermochemical power plants, Renew. Energy. 133 (2019) 770–786. doi:10.1016/J.RENENE.2018.10.071.

[23] E. Bagherisereshki, J. Tran, F. Lei, N. AuYeung, Investigation into SrO/SrCO 3 for high temperature thermochemical energy storage, Sol. Energy. 160 (2018) 85–93. doi:10.1016/j.solener.2017.11.073.

[24] N.R. Rhodes, A. Barde, K. Randhir, L. Li, D.W. Hahn, R. Mei, J.F. Klausner, N. AuYeung, Solar Thermochemical Energy Storage Through Carbonation Cycles of SrCO 3 /SrO Supported on SrZrO 3, ChemSusChem. 8 (2015) 3793–3798. doi:10.1002/cssc.201501023.

[25] F. Miccio, A.N. Murri, E. Landi, High-Temperature Capture of CO2 by Strontium Oxide Sorbents, Ind. Eng. Chem. Res. 55 (2016) 6696–6707. doi:10.1021/acs.iecr.6b00184.

[26] R. Perry, D. Green, Perry's Chemical Engineers' Handbook, 6th edn, McGraw-Hill, New York. 6 (1997) 641–672. http://highered.mcgraw-hill.com/sites/dl/free/0072849606/315014/physical_properties_table.pdf%5Cnhttp://scholar.google.com/scholar?hl=en&btnG=Search&q=intitle:Perry's+Chemical+Engineers'+Handbook,+6th#1.

[27] M. Broda, A.M. Kierzkowska, C.R. Müller, Influence of the Calcination and Carbonation Conditions on the CO 2 Uptake of Synthetic Ca-Based CO 2 Sorbents, Environ. Sci. Technol. 46 (2012) 10849–10856. doi:10.1021/es302757e.

[28] M. Gigantino, D. Kiwic, A. Steinfeld, Thermochemical energy storage via isothermal carbonation-calcination cycles of MgO-stabilized SrO in the range of 1000–1100 °C, Sol. Energy. 188 (2019) 720–729. doi:10.1016/j.solener.2019.06.046.

[29] F. Miccio, F. Doghieri, E. Landi, Insights into High Temperature Sorbents for Carbon Dioxide, Chem. Eng. Trans. 43 (2015) 901–906. doi:10.3303/CET1543151.

[30] P. Ammendola, F. Raganati, F. Miccio, A.N. Murri, E. Landi, Insights into utilization of strontium carbonate for thermochemical energy storage, Renew. Energy. 157 (2020) 769–781. doi:10.1016/j.renene.2020.05.048.

[31] L. Fedunik-Hofman, A. Bayon, S.W. Donne, Kinetics of Solid-Gas Reactions and Their Application to Carbonate Looping Systems, Energies. 12 (2019) 2981. doi:10.3390/en12152981.

[32] C. Ortiz, J.M. Valverde, R. Chacartegui, L.A. Perez-Maqueda, Carbonation of Limestone Derived CaO for Thermochemical Energy Storage: From Kinetics to Process Integration in Concentrating Solar Plants, ACS Sustain. Chem. Eng. 6 (2018) 6404–6417. doi:10.1021/acssuschemeng.8b00199.

[33] J. Sun, M.F. Bertos, S.J.R. Simons, Kinetic study of accelerated carbonation of municipal solid waste incinerator air pollution control residues for sequestration of flue gas CO 2, Energy Environ. Sci. 1 (2008) 370–377. doi:10.1039/b804165m.

[34] L. Rouchon, L. Favergeon, M. Pijolat, Analysis of the kinetic slowing down during carbonation of CaO by CO2, J. Therm. Anal. Calorim. 113 (2013) 1145–1155. doi:10.1007/s10973-013-2950-5.

[35] D. Lee, An apparent kinetic model for the carbonation of calcium oxide by carbon dioxide, Chem. Eng. J. 100 (2004) 71–77. doi:10.1016/j.cej.2003.12.003.

[36] S.K. Bhatia, D.D. Perlmutter, Effect of the product layer on the kinetics of the CO2-lime reaction, AIChE J. 29 (1983) 79–86. doi:10.1002/aic.690290111.

[37] P. Sun, J.R. Grace, C.J. Lim, E.J. Anthony, Determination of intrinsic rate constants of the CaO–CO2 reaction, Chem. Eng. Sci. 63 (2008) 47–56. doi:10.1016/j.ces.2007.08.055.

[38] M. Ramezani, P. Tremain, E. Doroodchi, B. Moghtaderi, Determination of Carbonation/Calcination Reaction Kinetics of a Limestone Sorbent in low CO2 Partial Pressures Using TGA Experiments, Energy Procedia. 114 (2017) 259–270. doi:10.1016/j.egypro.2017.03.1168.

[39] A. Di Giuliano, K. Gallucci, P.U. Foscolo, Determination of Kinetic and Diffusion Parameters Needed to Predict the Behavior of CaO-Based CO2 Sorbent and Sorbent-Catalyst Materials, Ind. Eng. Chem. Res. 59 (2020) 6840–6854. doi:10.1021/acs.iecr.9b05383.

[40] K. Kyaw, M. Kubota, F. Watanabe, H. Matsuda, M. Hasatani, Study of Carbonation of CaO for High Temperature Thermal Energy Storage., J. Chem. Eng. Japan. 31 (1998) 281–284. doi:10.1252/jcej.31.281.

[41] D. Alvarez, J.C. Abanades, Determination of the Critical Product Layer Thickness in the Reaction of CaO with CO2, Ind. Eng. Chem. Res. 44 (2005) 5608–5615.

[42] A. Khawam, D.R. Flanagan, Solid-state kinetic models: Basics and mathematical fundamentals, J. Phys. Chem. B. 110 (2006) 17315–17328. doi:10.1021/jp062746a.

[43] W. Ashraf, J. Olek, Carbonation activated binders from pure calcium silicates: Reaction kinetics and performance controlling factors, Cem. Concr. Compos. 93 (2018) 85–98. doi:10.1016/j.cemconcomp.2018.07.004.

[44] C.J. Goodbrake, J.F. Young, R.L. Berger, Reaction of Beta-Dicalcium Silicate and Tricalcium Silicate with Carbon Dioxide and Water Vapor, J. Am. Ceram. Soc. 62 (1979) 168–171. doi:10.1111/j.1151-2916.1979.tb19046.x.

[45] F. Raganati, M. Alfe, V. Gargiulo, R. Chirone, P. Ammendola, Kinetic study and breakthrough analysis of the hybrid physical/chemical CO2 adsorption/desorption behavior of a magnetite-based sorbent, Chem. Eng. J. 372 (2019) 526–535. doi:10.1016/j.cej.2019.04.165.

[46] Z. Li, F. Fang, X. Tang, N. Cai, Effect of Temperature on the Carbonation Reaction of CaO with CO2, Energy & Fuels. 26 (2012) 2473–2482. doi:10.1021/ef201543n.

[47] Y.A. Criado, B. Arias, J.C. Abanades, Effect of the Carbonation Temperature on the CO2 Carrying Capacity of CaO, Ind. Eng. Chem. Res. 57 (2018) 12595–12599. doi:10.1021/acs.iecr.8b02111.

[48] Z. Li, H. Sun, N. Cai, Rate equation theory for the carbonation reaction of CaO with CO 2,

Energy and Fuels. 26 (2012) 4607–4616. doi:10.1021/ef300607z.

[49] A. Biasin, C.U. Segre, M. Strumendo, CaCO3 Crystallite Evolution during CaO Carbonation: Critical Crystallite Size and Rate Constant Measurement by In-Situ Synchrotron Radiation X-ray Powder Diffraction, Cryst. Growth Des. 15 (2015) 5188–5201. doi:10.1021/acs.cgd.5b00563.

[50] S. Stendardo, L.K. Andersen, C. Herce, Self-activation and effect of regeneration conditions in CO2-carbonate looping with CaO-Ca12Al14O33 sorbent, Chem. Eng. J. 220 (2013) 383–394. doi:10.1016/j.cej.2013.01.045.

[51] P. Sun, J.R. Grace, C.J. Lim, E.J. Anthony, The effect of CaO sintering on cyclic CO2 capture in energy systems, AIChE J. 53 (2007) 2432–2442. doi:10.1002/aic.11251.

[52] P. Sun, C.J. Lim, J.R. Grace, Cyclic CO2 capture by limestone-derived sorbent during prolonged calcination/carbonation cycling, AIChE J. 54 (2008) 1668–1677. doi:10.1002/aic.11491.

[53] M. Zhao, X. He, G. Ji, Y. Song, X. Zhao, Zirconia incorporated calcium looping absorbents with superior sintering resistance for carbon dioxide capture from *in situ* or *ex situ* processes, Sustain. Energy Fuels. 2 (2018) 2733–2741. doi:10.1039/C8SE00413G.

[54] M. Zhao, M. Bilton, A.P. Brown, A.M. Cunliffe, E. Dvininov, V. Dupont, T.P. Comyn, S.J. Milne, Durability of CaO-CaZrO3 sorbents for high-temperature CO 2 capture prepared by a wet chemical method, Energy and Fuels. 28 (2014) 1275–1283. doi:10.1021/ef4020845.

[55] V. Manovic, E.J. Anthony, Lime-Based Sorbents for High-Temperature CO2 Capture—A Review of Sorbent Modification Methods, Int. J. Environ. Res. Public Health. 7 (2010) 3129–3140. doi:10.3390/ijerph7083129.

[56] V. Manovic, E.J. Anthony, Thermal activation of CaO-based sorbent and self-reactivation

during CO2 capture looping cycles., Environ. Sci. Technol. 42 (2008) 4170–4. http://www.ncbi.nlm.nih.gov/pubmed/18589983.

[57] L. Fedunik-Hofman, A. Bayon, S.W. Donne, Comparative kinetic analysis of CaCO3/CaO reaction system for energy storage and carbon capture, Appl. Sci. 9 (2019) 5–9. doi:10.3390/app9214601.

[58] M.H. Sedghkerdar, E. Mostafavi, N. Mahinpey, Investigation of the Kinetics of Carbonation Reaction with Cao-Based Sorbents Using Experiments and Aspen Plus Simulation, Chem. Eng. Commun. 202 (2015) 746–755. doi:10.1080/00986445.2013.871709.

[59] J. Yin, C. Qin, B. Feng, L. Ge, C. Luo, W. Liu, H. An, Calcium Looping for CO 2 Capture at a Constant High Temperature, Energy & Fuels. 28 (2014) 307–318. doi:10.1021/ef401399c.

Nomenclature

E	activation energy of the intrinsic kinetic rate of the fast carbonation reaction
f(α)	reaction kinetic model
g(α)	integral form of the reaction kinetic model
h	thickness of the $SrCO_3$ product layer at the transition between the fast and slow reaction periods
k_0	pre-exponential factor of the intrinsic kinetic rate of the fast carbonation reaction
ks	intrinsic kinetic constant of the fast kinetically controlled stage
r	apparent carbonation reaction rate
m	sample mass
M_{SrO}	molecular weights of SrO
M_{CO2}	molecular weights of CO_2
P_{CO_2}	CO_2 partial pressure
$P_{CO_2}^{eq}$	equilibrium CO_2 partial pressure
S_0	SrO specific surface per unit mass
t	time
X_{SrO}	SrO carbonation conversion degree
X_u	ultimate carbonation conversion degree
$V_{SrCO_3}^M$	$SrCO_3$ molar volume

w	mass fraction of SrO in the sample

Greek letters

α	extent of carbonation conversion
Δm	weight variation of the sample during carbonation

Kinetics of the Carbonation Reaction of an $SrO-Al_2O_3$ Composite for Thermochemical Energy Storage

Paola Ammendola[a], Federica Raganati[a,*], Elena Landi[b], Annalisa Natali Murri[b], Francesco Miccio[b]

[a]Istituto di Scienze e Tecnologie per l'Energia e la Mobilità Sostenibili (STEMS) - CNR, Piazzale Tecchio 80, 80125 Naples, Italy

[b]Istituto di Scienza e Tecnologia dei Materiali Ceramici (ISTEC) - CNR, via Granarolo, 64, 48018 Faenza, Italy

Supplementary Material

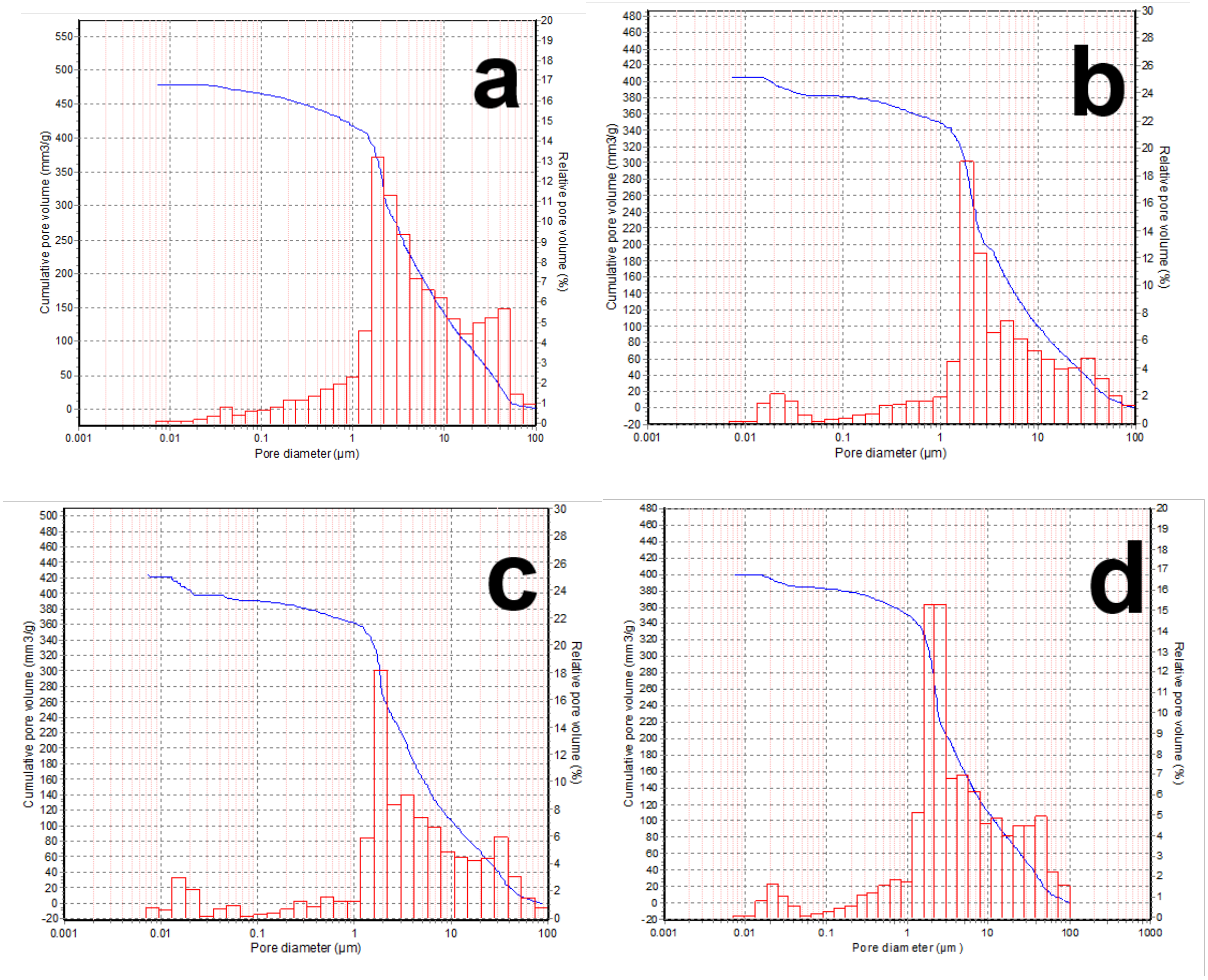

Fig. S1. Pore size distribution of the fresh (a) SrO-Al_2O_3 composite sample and of the cycled composite samples at (b) 900, (c) 1000 and (d) 1050 °C.

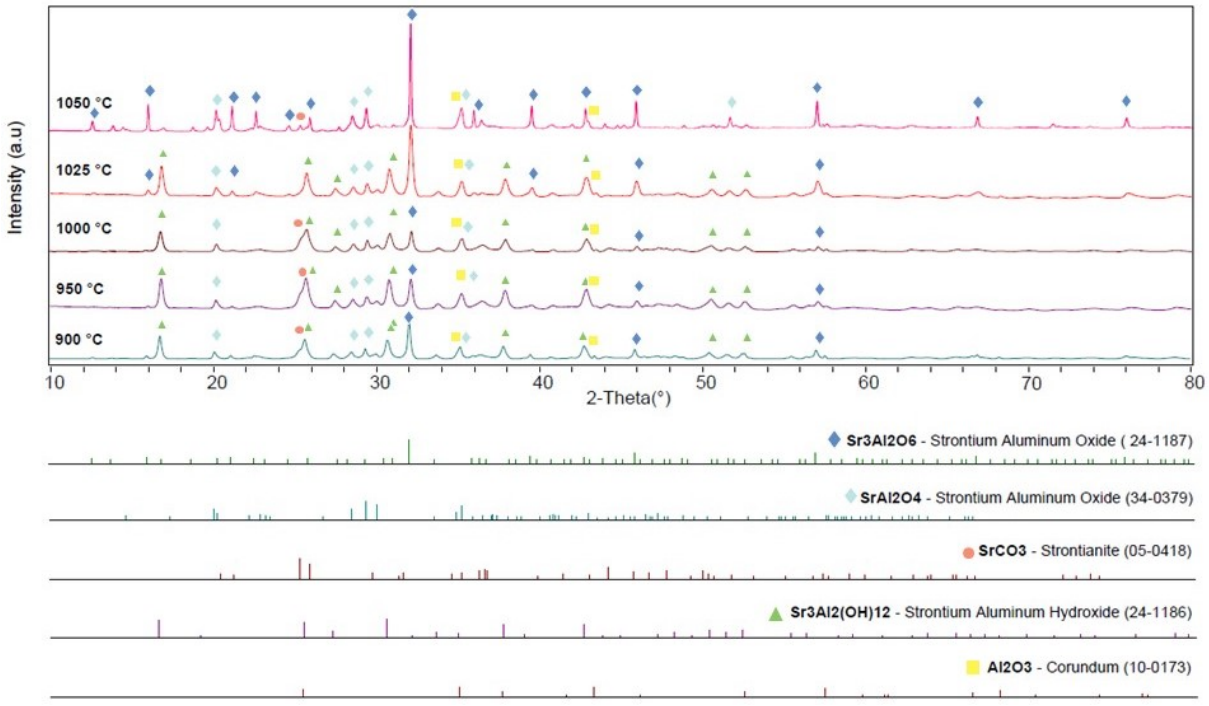

Fig. S2. XRD analysis the SrO-Al_2O_3 composite samples cycled at the different investigated temperatures.

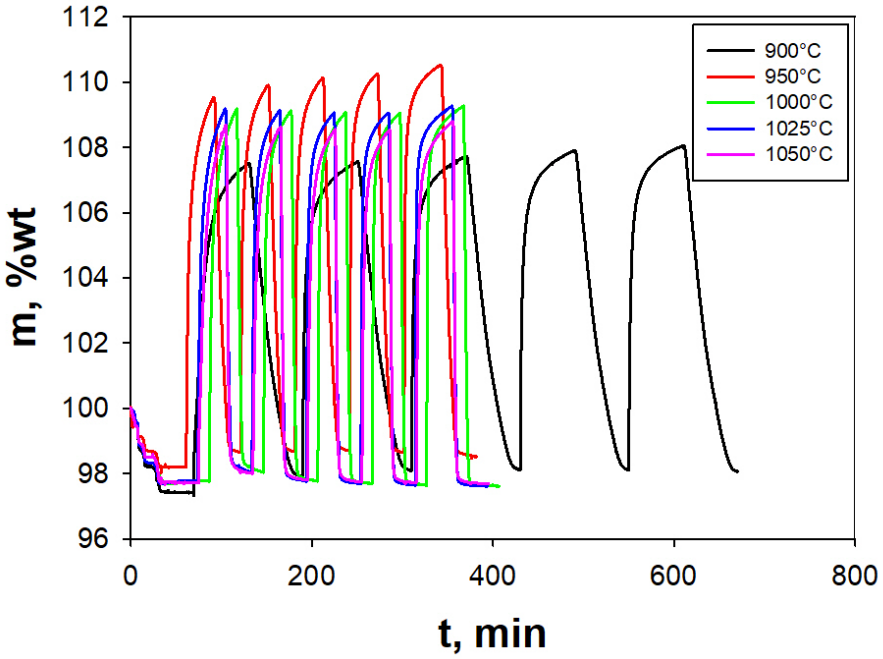

Fig. S3. TGA cycles of the SrO-Al_2O_3 composite at different temperatures.